RSC Advances

PAPER

View Article Online
View Journal | View Issue

Cite this: *RSC Adv.*, 2026, **16**, 22784

Valorization of $BaCO_3$ with 8-HQS to produce the optical chemo-probe for highly selective sensing of Cd^{2+} in aqueous media

Sahel Sharifi,[a] Amin Moghaddasfar,[a] Ghodsi Mohammadi Ziarani[b] and Alireza Badiei*[a]

Received 5th February 2026
Accepted 3rd April 2026

DOI: 10.1039/d6ra01012a

rsc.li/rsc-advances

Valorization of chemicals is considered a method to prevent loss of valuable substances. Barium carbonate, as an initial precursor in chemical industries, is a suitable candidate for valorization to prevent the accumulation of waste $BaCO_3$ and the loss of these valuable resources. In this study, $BaCO_3$ was valorized with 8-hydroxyquinoline-5-sulfonate (8-HQS) to produce the optical chemo-probe for highly selective sensing of Cd^{2+} in aqueous media. The emission intensity of $BaCO_3$-8-HQS was enhanced in the presence of Cd^{2+} at 520 nm (λ_{ex} = 392 nm). The electrochemical experimental investigation, including cyclic voltammetry and Mott–Schottky techniques, revealed the ICT-enhancing mechanism of Cd^{2+} and showed Cd^{2+} interacts with the sulfonate head of $BaCO_3$-8-HQS. Furthermore, the as-prepared $BaCO_3$-8-HQS exhibited a good affinity and selectivity for sensing Cd^{2+}, with a limit of detection of 2.2×10^{-7} M.

Introduction

Valorization refers to converting waste into high-value-added materials. One of the main challenges in recycling is the intricate process of separating waste into usable secondary raw materials. To tackle this important topic, tight controls on waste management and substantial investments in waste materials, valorization are being introduced. In this context, the idea of recycling and reusing waste to produce valuable products has inspired researchers to use waste for various applications.[1–3] Nowadays, the industrial revolution has entered a fast-paced stage, leading to numerous developments. Consequently, through the industry's process, large amounts of precursors as industry raw materials can remain unusable or wasted. In this regard, the valorization of raw materials has been considered a sustainable method to obtain various high-value-added materials.[4–6] Among these materials, barium carbonate stands out as a promising candidate for valorization due to its low cost, availability, and abundance as an inorganic compound.

Barium is a white alkaline metal that exists in two forms: sulfate and carbonate. $BaCO_3$, also known as witherite, offers several significant advantages. In industry, barium carbonate is normally produced from barite and is enormously favorable for many applications in glass manufacturing, oil drilling, photography, ceramics, paint, brick production, and chemical processes.[7,8] However, in some industries and university laboratories, large quantities of $BaCO_3$ have gone to waste over the years.[9] By valorization of this waste, $BaCO_3$ can be reused, reducing waste and contributing to sustainable development.

In recent years, drinking water pollution has become a significant issue that poses a threat to human society.[10–12] As a common heavy metal pollutant, cadmium ions (Cd^{2+}) are well-known for their detrimental effects on food safety, ecosystems,

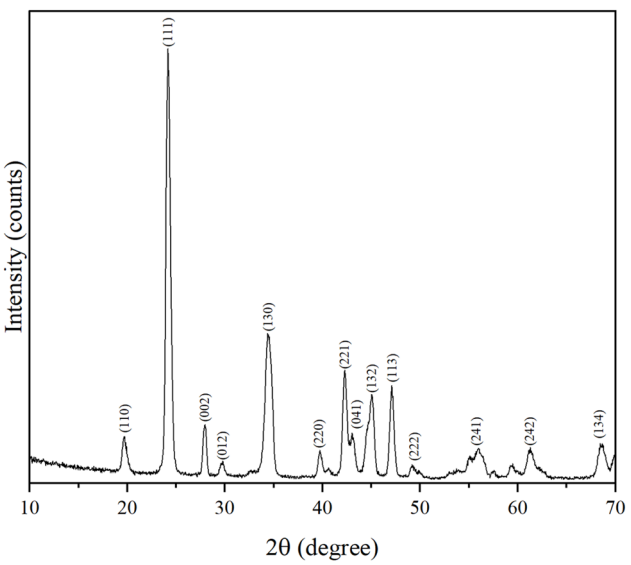

Fig. 1 XRD pattern of $BaCO_3$.

[a]School of Chemistry, College of Sciences, University of Tehran, Iran. E-mail: abadiei@ut.ac.ir

[b]Department of Organic Chemistry, Faculty of Chemistry, Alzahra University, Iran

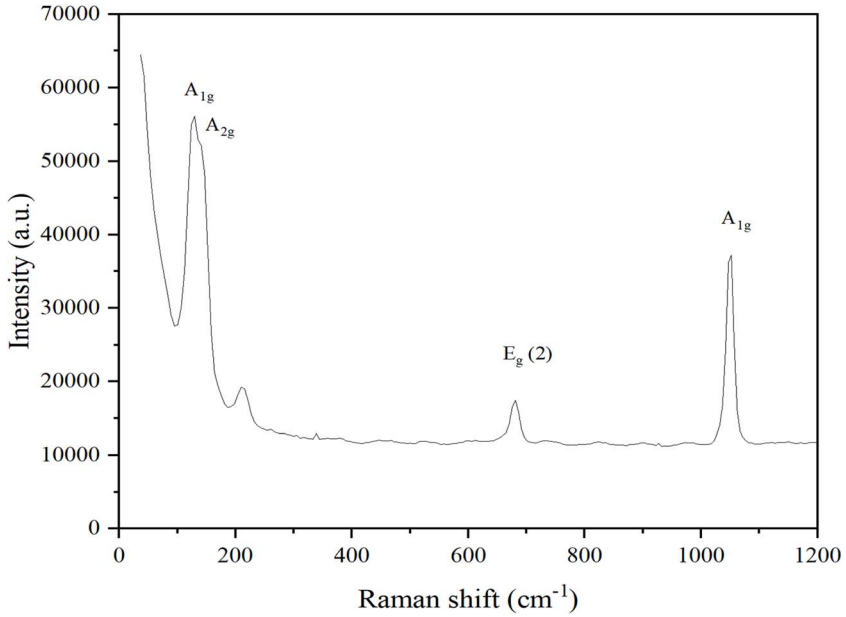

Fig. 2 Raman spectrum of $BaCO_3$.

and human health. High concentrations of Cd^{2+} are highly toxic and can cause serious disasters.[13,14] Traditional detection methods require skilled technicians, expensive instruments, and complex sample pretreatment, which limits their wide applications in routine testing.[15–18] In this context, the development of optical chemo probes has garnered significant scientific attention. Optical chemo probes have successfully addressed these drawbacks, offering cost-effectiveness, high selectivity and sensitivity, instantaneous response, and operational simplicity.[19–24] The notable fluorescence characteristics of 8-hydroxyquinoline (8-HQ) and its derivatives highlight their potential for developing selective and highly sensitive fluorescent chemo-sensors. Known as a chelating agent, 8-HQ exhibits weak fluorescence mainly due to a non-radiative relaxation mechanism linked to intramolecular proton transfer (from the oxygen to the nitrogen of 8-HQ) in its excited state. When 8-HQ interacts with metal ions, the metal ion can replace the hydroxyl proton, thereby inhibiting the intramolecular proton transfer. Consequently, the binding of metal ions to 8-HQ can lead to a significant alteration in fluorescence intensity.[25] 8-Hydroxyquinoline-5-sulfonate (8-HQS) is a derivative of 8-HQ, a widespread moiety due to excellent properties for the formation of complexes with different metal ions and anions. Also, it

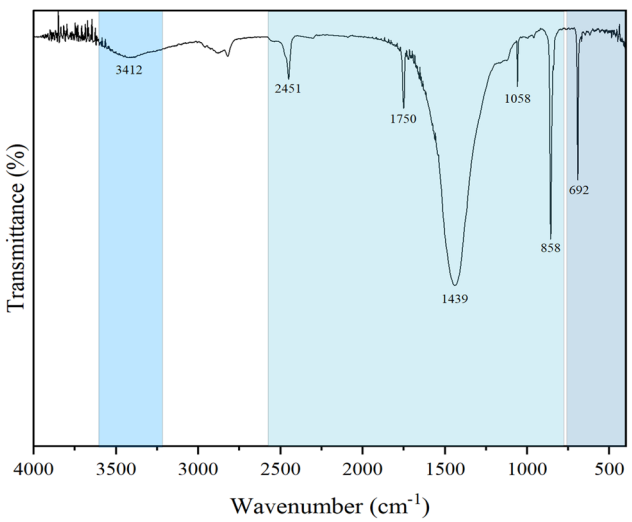

Fig. 3 FTIR spectrum of $BaCO_3$.

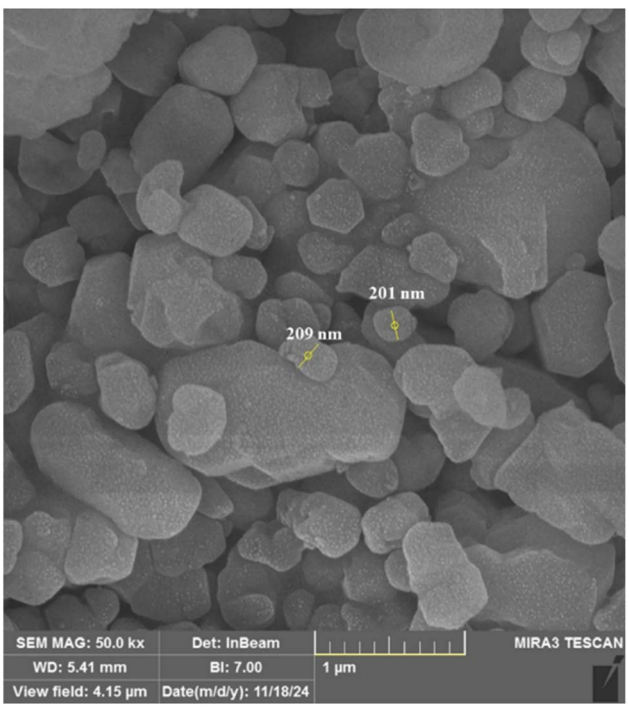

Fig. 4 SEM image of $BaCO_3$.

Table 1 Zeta potential of $BaCO_3$ and $BaCO_3$-8-HQS

Sample	Zeta potential (mV)
$BaCO_3$	−0.3
$BaCO_3$-8-HQS	−22.4

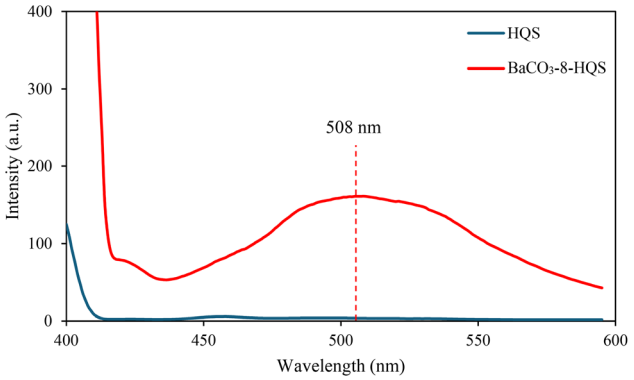

Fig. 5 Fluorescence spectra of HQS and $BaCO_3$-8-HQS.

can act as a fluorophore ligand in complex formations with transition metal ions.[26] The interaction between barium carbonate and 8-HQS will lead to an optical chemo probe.

Herein, to the best of our knowledge, $BaCO_3$ has been valorized with 8-HQS to produce the optical chemo probe for the first time. The as-prepared optical probe shows high affinity to probe Cd^{2+} with high sensitivity (limit of detection (LoD) = 2.2 × 10^{-7} M) in aqueous media. The result showed a remarkable enhancement of emission intensity for sensing Cd^{2+}. The $BaCO_3$-8-HQS was characterized by photoluminescence (PL), Mott–Schottky analysis, cyclic voltammetry, and zeta potential. These techniques were used to evaluate PL properties, electronic characteristics, and surface charge, respectively.

Chemicals

8-Hydroxyquinoline sulfonic acid ($C_9H_7NO_4$, ≥98% purity) was obtained from Sigma-Aldrich. The following ions were investigated in aqueous solutions: K^+, Ag^+, Hg^+, Cu^{2+}, Ni^{2+}, Cr^{3+}, Zn^{2+}, Co^{2+}, Pb^{2+}, Ca^{2+}, Cd^{2+}, Hg^{2+}, Mn^{2+}, Fe^{3+}, and Al^{3+}. Analytical-grade metal salts, either chlorides or nitrates, were used to prepare the stock solutions. All materials were used as analytical grade, without any further purification.

Synthesis of $BaCO_3$-8-HQS

In an undergraduate inorganic chemistry laboratory class, $BaCO_3$ was synthesized through the aqueous titration of barium chloride with sodium carbonate. Unfortunately, it was

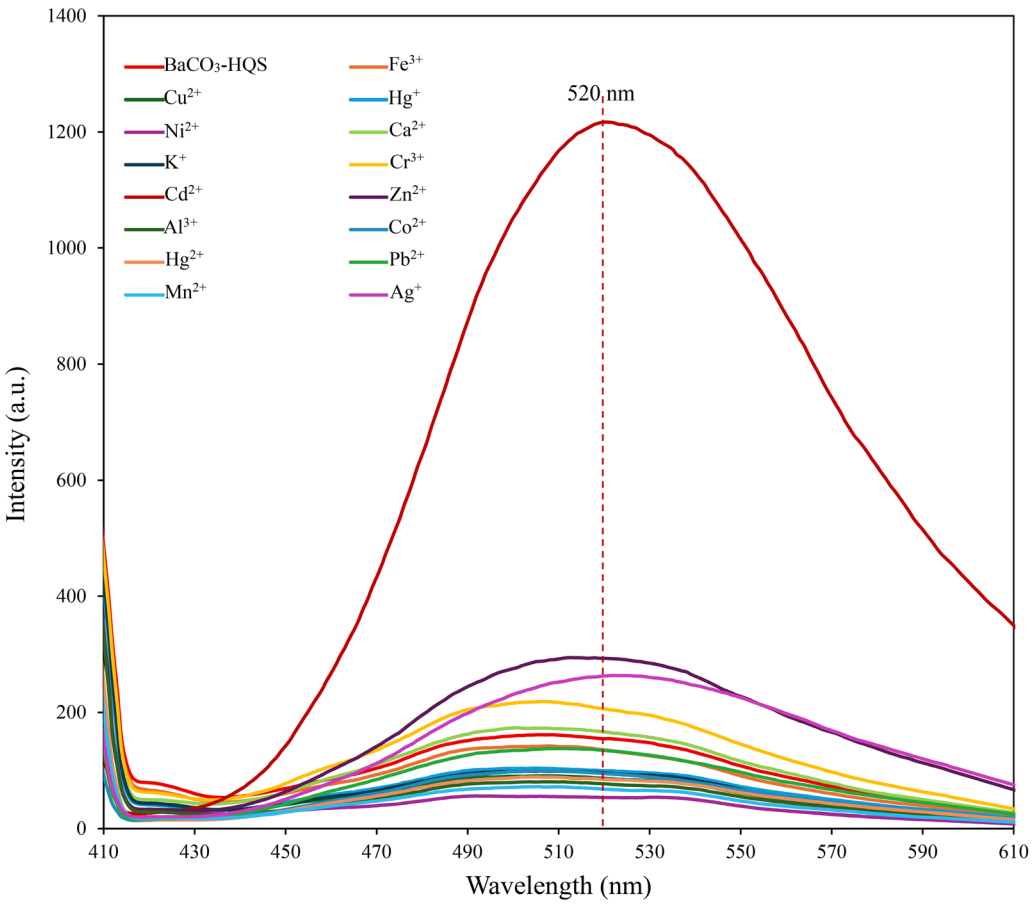

Fig. 6 Fluorescence spectra of $BaCO_3$-8-HQS in the presence of various metal ions in aqueous solution (λ_{ex} = 392 nm).

discarded at the end of the experiment. This study utilized the wasted $BaCO_3$ to illustrate the concept of waste valorization. For the preparation of $BaCO_3$-8-HQS, 0.01 g of $BaCO_3$ was dispersed in 50 mL of deionized water and stirred for 1 h. Then, 8-HQS (0.01 g) was introduced to it and sonicated for 20 min.

Characterization of $BaCO_3$

The crystal phase pattern of $BaCO_3$ was investigated by powder X-ray diffraction (XRD) with Cu Kα irradiation in the 2θ range of 10–80° (Rigaku Ultima IV). Fourier transform infrared spectroscopy (FT-IR), Rayleigh WQF-510A, was utilized to examine the structure of the $BaCO_3$ in the range of 400–4000 cm^{-1}. Raman spectroscopy was utilized to investigate crystalline structure stability with the Teskan N1-541 instrument. The fluorescence spectra were used at ambient temperature on an Agilent-G980A spectrofluorometer. A Raleigh UV-1600 spectrophotometer was used for UV-vis spectroscopy studies. The morphology of $BaCO_3$ was investigated by scanning electron microscopy (MIRA3-Tescan). Zeta potential data were collected by Horiba SZ-100 to examine the surface charge. The Mott–Schottky (M–S) analysis and cyclic voltammetry (CV) were performed using an Ivium Vertex with a 0.1 M Na_2SO_4 electrolyte solution. The M–S analysis was conducted at a frequency of 1467.8 Hz.

Results and discussion

The powder X-ray diffractometry has been utilized to analyze the crystallographic phases. Fig. 1 depicts the obtained XRD pattern of the prepared sample. In the XRD pattern of $BaCO_3$, the diffractions located at 19.72°, 24.16°, 27.94°, 29.79°, 34.43°, 39.74°, 42.26°, 43.03°, 45.04°, 47.09°, 49.16°, 55.93°, 61.24°, and 68.55° can be respectively assigned to the (110), (111), (002), (012), (130), (220), (221), (041), (132), (113), (222), (241), (242), and (134) planes of the $BaCO_3$ crystalline structure.[27] According to the Scherrer equation, which is given in eqn (1), the average crystallite size of $BaCO_3$ was calculated and obtained as 21.54 nm.

$$D = \frac{k\lambda}{\beta \cos \theta} \quad (1)$$

Raman spectroscopic analysis has been utilized to get a deep understanding of the crystalline structural stability of as-prepared $BaCO_3$. Fig. 2 illustrates that the as-prepared $BaCO_3$

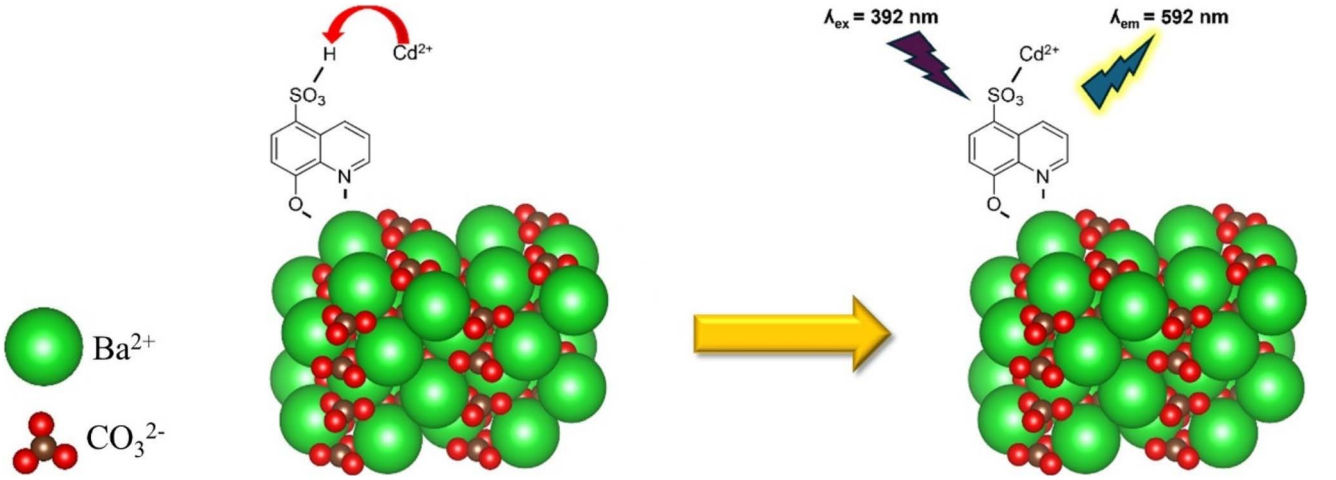

Scheme 1 The feasible interaction pathway between $BaCO_3$-8-HQS and Cd^{2+}.

Table 2 Performance comparison of reported studies for sensing Cd^{2+}

Sensor	LoD (μM)	Measured signal	Ref.
(*E*)-4-((2-(2,4-Dinitrophenyl)hydrazineylidene)methyl)-*N*,*N* dimethyl-aniline	0.0756	Fluorescence	31
5-(4-(Dimethylamino)phenyl)-3-(2-hydroxyphenyl)-4,5-dihydro-1*H*-pyrazole-1-carbothioamide	0.8158	Fluorescence	32
Hydroxy-naphthaldehyde and tris(2-aminoethyl)amine (TREN)	0.0678	Fluorescence	33
5-(4′-([2,2′:6′,2″-Terpyridin]−4′-yl)-[1,1′-biphenyl]4-yl)7,8,13,14-tetrahydrodibenzo [*a*, *i*] phenanthridine (TBTP)	0.01181	Fluorescence	34
GTAuNPs	0.025	Fluorescence	35
GSH-AuNPs	0.0188	Fluorescence	36
N, B-CQDs	0.45	Fluorescence	37
AgInZnS QDs	0.0378	Fluorescence	38
Eu-MOF	0.00991	Fluorescence	39
$BaCO_3$-8-HQS	0.224	Fluorescence	This study

has the signature of internal CO_3 Raman bands at 1054 $cm^{-1}(A_{1g})$ and 686 cm^{-1} $(E_g(2))$, which belong to symmetric stretching (υ_1) and in-plane bending (υ_2), respectively. Furthermore, the prepared sample has a couple of strong lattice Raman bands at 149 and 130 cm^{-1} that belong to A_{2g} and A_{1g} Raman bands, respectively.[28]

Fig. 3 illustrates the FT-IR spectrum of the as-prepared sample. The peaks at 1058 cm^{-1} and 1439 cm^{-1} might be due to the symmetric vibration of $\upsilon_s[COO^-]$ and the asymmetric vibration of $\upsilon_{as}[COO^-]$, respectively. In the fingerprint region, the $BaCO_3$ peak could be observed at 692 cm^{-1}; the out-of-plane bending appears at 858 cm^{-1} and the overtone/combination band is observed at 1750 cm^{-1}.[29,30] The peak at 3412 cm^{-1} is characteristic of the O–H bond.

Fig. 4 shows the SEM images depicting the morphology of $BaCO_3$. The particle size of $BaCO_3$ was calculated by the digimizer software and obtained as approximately 205 nm. The zeta potential of the $BaCO_3$-8-HQS and $BaCO_3$ samples was investigated. The zeta potential also confirms the interaction between 8-HQS and $BaCO_3$ (Fig. S1). According to the result, the zeta potential was −0.3 and −22.4 mV for $BaCO_3$ and $BaCO_3$-8-HQS, respectively (Table 1). Based on the zeta potential results, 8-HQS interacts with $BaCO_3$ through its nitrogen and oxygen atoms, while the sulfonic acid head remains free. Consequently, the zeta potential increases after the interaction of $BaCO_3$ with 8-HQS.

The photoluminescence properties of 8-HQS and $BaCO_3$-8-HQS were investigated to confirm the interaction of 8-HQS and $BaCO_3$ (Fig. 5). The result clearly demonstrates the successful interaction of $BaCO_3$ with 8-HQS. The excitation wavelength (λ_{ex}) was set to 392 nm for PL analysis. 8-HQS did not illustrate any emission intensity, but after introducing $BaCO_3$, its emission intensity was enhanced at 508 nm.

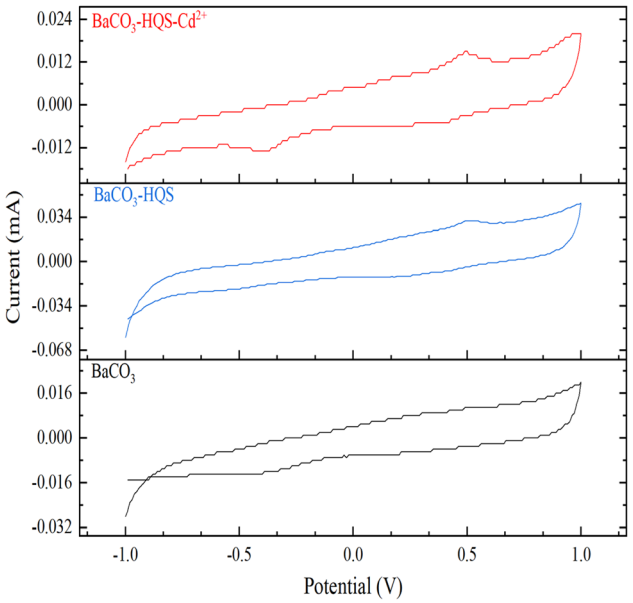

Fig. 8 The cyclic voltammetry (CV) plots for three conditions: the $BaCO_3$, $BaCO_3$-8-HQS, and $BaCO_3$-8-HQS in the presence of Cd^{2+}.

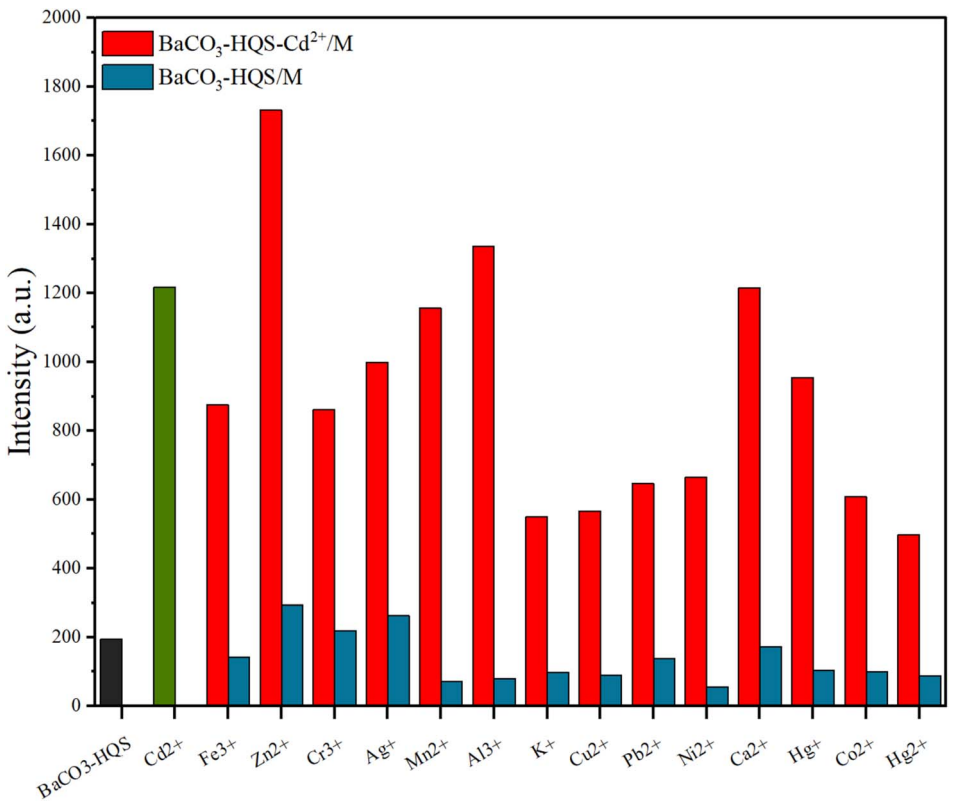

Fig. 7 The emission intensity of $BaCO_3$-8-HQS in the presence of Cd^{2+} and interfering species.

Photoluminescence examination

The PL behavior of $BaCO_3$-8-HQS was investigated in the presence of a broad range of metal ions, including K^+, Ag^+, Hg^+, Cu^{2+}, Ni^{2+}, Cr^{3+}, Zn^{2+}, Co^{2+}, Pb^{2+}, Ca^{2+}, Cd^{2+}, Hg^{2+}, Mn^{2+}, Fe^{3+}, and Al^{3+}. For the PL investigation, 5 μL of a desired concentration of metal ion (0.01 M) was added to 2 mL of $BaCO_3$-8-HQS, and then the entire sample was transferred into a cuvette. Fig. 6 illustrates the sensing results of the $BaCO_3$-8-HQS with these metal ions. According to the results, adjusting the excitation wavelength to 392 nm slightly enhanced the emission intensity of BaCO3-8-HQS in the presence of Ag^+, Ca^{2+}, Cr^{3+}, and Zn^{2+}. However, the emission intensity was quenched in the presence of other metal ions. Notably, upon the addition of Cd^{2+}, emission intensity significantly increased, accompanied by a red shift to 520 nm. Scheme 1 illustrates the proposed interaction pathway between $BaCO_3$-8-HQS and Cd^{2+} through optical chemo sensing. For LoD determination of Cd^{2+}, the as-prepared $BaCO_3$-8-HQS was titrated with a design concentration of Cd^{2+} (Fig. S2). The LoD for sensing Cd^{2+} was obtained as 2.2 ч 10^{-7} M. Table 2 shows the compression of different optical chemo-sensors to probe Cd^{2+}.

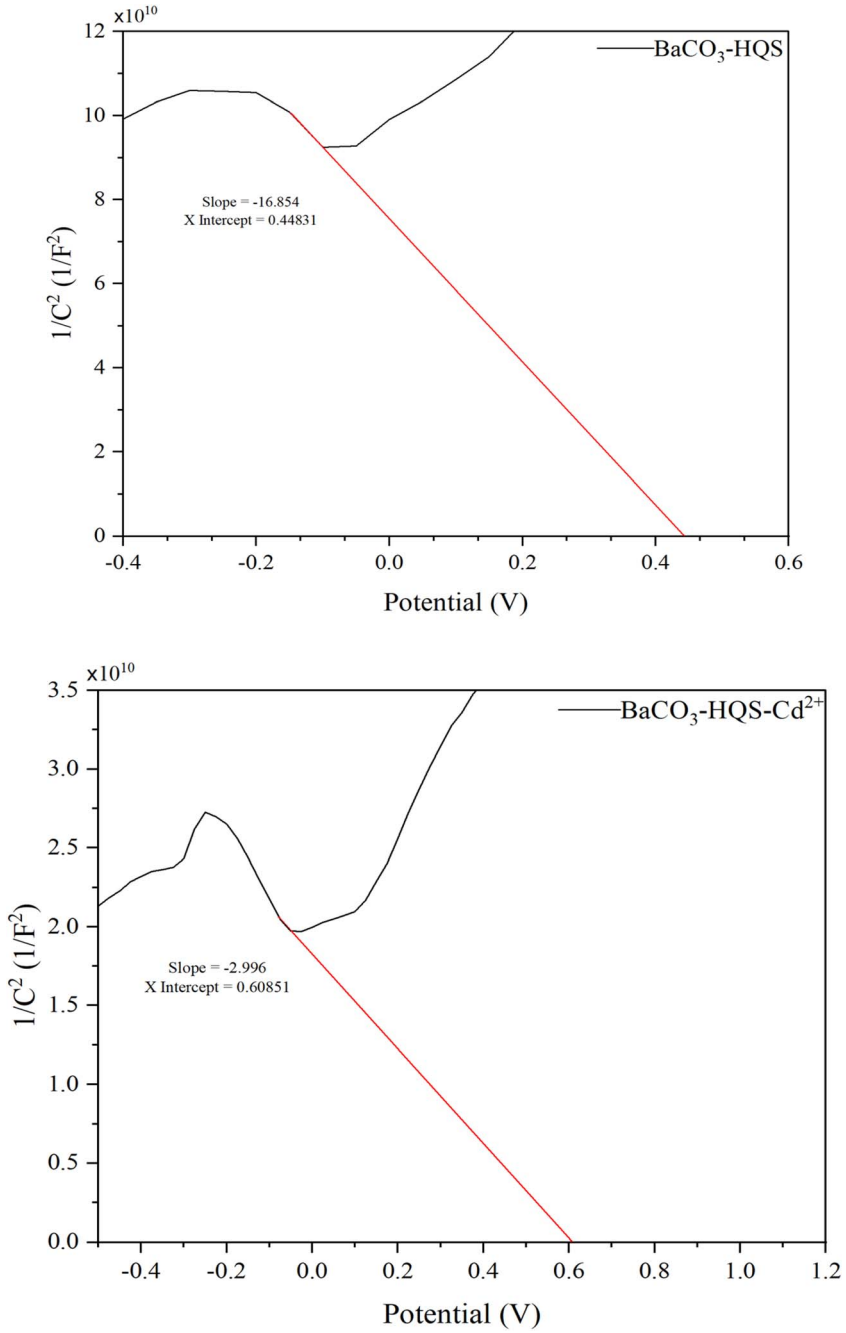

Fig. 9 Mott–Schottky plots for $BaCO_3$-8-HQS and $BaCO_3$-8-HQS+Cd^{2+} in a 0.1 m Na_2SO_4.

For the investigation of the selectivity and affinity of the as-prepared $BaCO_3$-8-HQS, the emission intensity was measured for detecting Cd^{2+} in the presence of interfering species (λ_{ex} = 392 nm). The results showed that the emission intensity of the $BaCO_3$-8-HQS + Cd^{2+} complex was not completely quenched by these interfering species (Fig. 7). Therefore, the $BaCO_3$-8-HQS demonstrated a high selectivity and stability for sensing Cd^{2+}.

Enhancing mechanism

According to the principles of intramolecular charge transfer (ICT) in view of receptors, within the same molecular framework, an electron-acceptor fragment is interconnected with an electron-donor fragment, leading to the establishment of a "push–pull" electronic condition in the excited state. The interaction of the electron-donating part with the analyte (such as a cation) leads to a reduction in the electron-donor capability of the prepared probe. This change results in a blue shift in the absorption spectrum of the sensor. Conversely, the interaction of the electron-accepting part with the analyte, leading to a hyperchromic shift, occurs in the absorption spectrum due to the predominant ICT. Furthermore, the ICT phenomenon may either be enhanced or constrained, leading to either a hyperchromic or hypsochromic shift in the PL properties of the probe.[40] To investigate the enhancing mechanism, UV-Vis spectroscopy and M–S analysis were utilized. M–S is used by a standard three-electrode electrochemistry method, including the working electrode (glassy carbon), counter electrode (the platinum wire), and reference electrode (Ag/AgCl). M–S analysis of $BaCO_3$, $BaCO_3$-8-HQS, and $BaCO_3$-8-HQS+Cd^{2+} samples was carried out in a 0.1 M Na_2SO_4 aqueous solution. To ensure results from the M–S analysis, CV analysis was performed to investigate the electrical properties of $BaCO_3$-8-HQS. According to Fig. 8, $BaCO_3$ shows no anodic or cathodic peaks in the CV. However, after the interaction with 8-HQS, anodic peak potentials appeared, and following the introduction of Cd^{2+}, both anodic and cathodic peaks were observed. According to the results, the bond gap potential of $BaCO_3$-8-HQS decreased after interaction of $BaCO_3$-8-HQS with Cd^{2+}. In the ICT-enhancing mechanism reviewed by Paul and co-authors,[41] it is noted that the analyte can interact with acceptor and donor heads, yielding different results in PL and UV-Vis spectroscopies. Therefore, determining the highest occupied molecular orbital (HOMO) energy level of the optical chemo probe before and after interaction with the analyte can show which part of the optical chemo probe interacts with the analyte. When the analyte interacts with the acceptor part, the HOMO energy level of the optical chemoprobe decreases. When the analyte interacts with the donor part, the HOMO energy level of the optical chemo probe increases. In this regard, M–S analysis was utilized to estimate this mechanism. For M–S measurements, the frequencies adjusted at 1467.8 Hz reveal the electronic characteristics of $BaCO_3$-8-HQS and $BaCO_3$-8-HQS+Cd^{2+}, with negative slopes illustrating the p-type nature of the electronic band

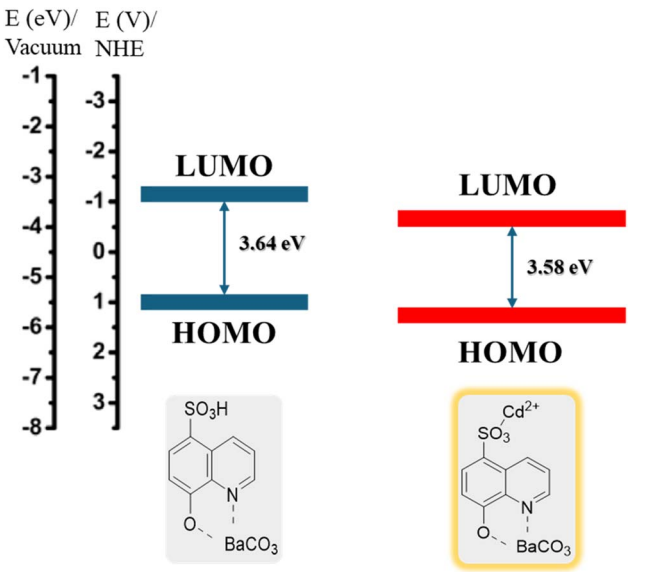

Fig. 10 Illustration of HOMO and LUMO energy levels of $BaCO_3$-8-HQS and $BaCO_3$-8-HQS + Cd^{2+}.

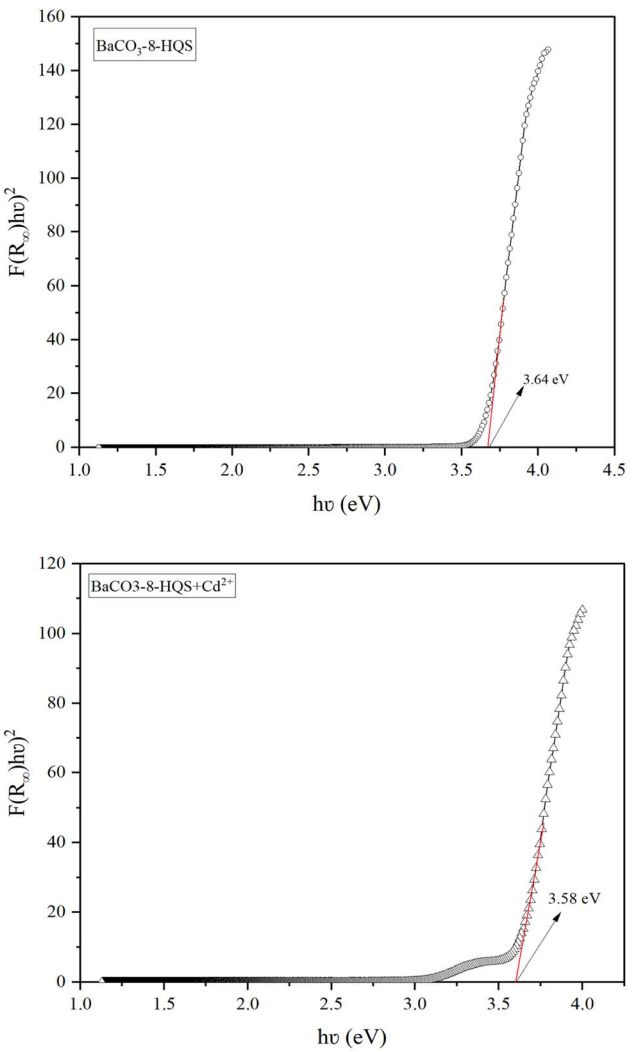

Fig. 11 Bond gap analysis of $BaCO_3$-8-HQS and $BaCO_3$-8-HQS + Cd^{2+} using Tauc equation.

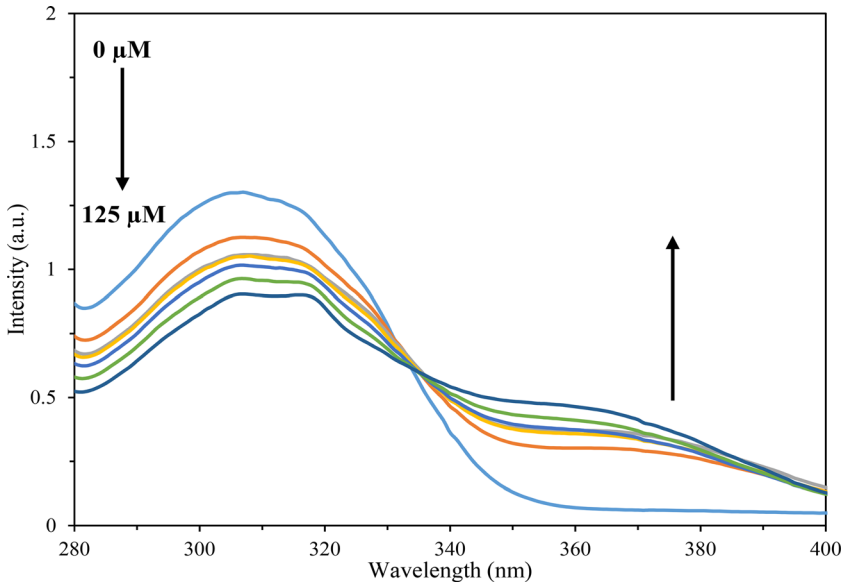

Fig. 12 UV-Vis absorption spectral changes through adding Cd^{2+} with varying concentrations.

structure (Fig. 9). The intersection point is the flat band position, examined from the intersection, which is 1.06 V (−5.56 eV) and 1.22 V (−5.72 eV) *versus* RHE for $BaCO_3$-8-HQS and $BaCO_3$-8-HQS+Cd^{2+}, respectively (Fig. 10), approximately corresponding to the HOMO. According to results, Cd^{2+} interacts with the acceptor part of $BaCO_3$-8-HQS, specifically with the sulfonate head of 8-HQS. For determining bond gap of $BaCO_3$-8-HQS and $BaCO_3$-8-HQS+Cd^{2+}, Tauc equation[42] was utilized to obtain bond gap and lowest unoccupied molecular orbital (LUMO). According to Fig. 11, the bond gaps of $BaCO_3$-8-HQS and $BaCO_3$-8-HQS+Cd^{2+} were determined to be 3.64 eV and 3.58 eV, respectively.

The UV-Vis spectroscopy was employed to investigate the effect of introducing Cd^{2+} ion into the as-prepared chemo probe suspension. The results showed that a little red shift was observed as the concentration of Cd^{2+} increased from 0 µM to 125 µM. Furthermore, this complexation of $BaCO_3$-8-HQS with Cd^{2+} resulted in the noted isosbestic point approximately at 335 nm (Fig. 12). According to the result, the enhancing mechanism is examined as an ICT.

pH effect examination

The environmental factors affecting optical chemo probes are crucial for the detection of analytes. Among these factors, the pH of the environment plays a significant role in sensory performance. In this context, the performance of the $BaCO_3$-8-HQS was investigated across a wide pH range. Fig. S3 clearly shows that the probe remains stable within a narrow pH range of 5 to 6. In harsh acidic conditions, the emission intensity is completely quenched. In the pH range of 7 to 10, the emission intensity decreases but stabilizes at a certain level. Based on the results obtained, the optimal pH range for the as-prepared optical probe for detecting Cd^{2+} is thus identified as 5 to 6.

Conclusion

In summary, this work represented the valorization of barium carbonate to a high-value-added compound based on an optical chemosensor as a low-cost and widely available material that did not require complex functionalization or energy-intensive synthesis. It is noteworthy that the $BaCO_3$-8-HQS demonstrates remarkable selectivity and good sensitivity for Cd^{2+} ions in aqueous media (LoD = 2.2×10^{-7} M). The enhancing mechanism of Cd^{2+} was experimentally determined as ICT and revealed that Cd^{2+} interacts with the sulfonate head of 8-HQS, which was investigated using the electrochemical techniques such as CV and M–S. According to the results, the HOMO energy level of $BaCO_3$-8-HQS and $BaCO_3$-8-HQS+Cd^{2+} was obtained as −5.56 eV and −5.72 eV *versus* RHE, respectively. Furthermore, the bond gap of $BaCO_3$-8-HQS and $BaCO_3$-8-HQS+Cd^{2+} were calculated using Tauc equation, yielding 3.64 eV and 3.58 eV, respectively. The development of this simple method can open a new path for the development of optical chemo probes, specifically with metal oxides, to selectively probe heavy metal ions in aqueous media.

Conflicts of interest

All authors declare that they have no conflicts of interest.

Data availability

The data which support the findings of this study are available from the corresponding author, upon request and also the data supporting this article have been included as part of the supplementary information (SI). Supplementary information is available. See DOI: https://doi.org/10.1039/d6ra01012a.

Acknowledgements

This work is based upon research funded by the Iran National Science Foundation (INSF) under project No.4038013.

References

1 S. Liu, M. Wang, Q. Cheng, Y. He, J. Ni, J. Liu, C. Yan and T. Qian, Turning waste into wealth: sustainable production of high-value-added chemicals from catalytic coupling of carbon dioxide and nitrogenous small molecules, *ACS Nano*, 2022, **16**, 17911–17930.

2 A. Rahimi and J. M. García, Chemical recycling of waste plastics for new materials production, *Nat. Rev. Chem.*, 2017, **1**, 0046.

3 D. D. Sarode, Use of industrial waste for value-added products, in S. Verma, R. Khan, M. Mili, S. A. R. Hashmi, A. K. Srivastava, *Advanced Materials from Recycled Waste*, Amsterdam, 2022, pp. 179–198.

4 R. A. D. Arancon, C. S. K. Lin, K. M. Chan, T. H. Kwan and R. Luque, Advances on waste valorization: new horizons for a more sustainable society, *Energy Sci. Eng.*, 2013, **1**, 53–71.

5 C. Xu, M. Nasrollahzadeh, M. Selva, Z. Issaabadi and R. Luque, Waste-to-wealth: biowaste valorization into valuable bio(nano)materials, *Chem. Soc. Rev.*, 2019, **48**, 4791–4822.

6 M. Panigrahi, R. I. Ganguly and R. R. Dash, Applications, challenges and opportunities of industrial waste resources ceramics, *High Electrical Resistance Ceramics - Thermal Power Plant Waste Resources*, Scrivener, Beverly, (2023), 181–197.

7 H. G. Emblem and K. Hargreaves, Preparation, Properties and Uses of Barium Compounds, *Rev. Inorg. Chem.*, 1995, **15**, 109–138.

8 P. Patnaik, *Handbook of Inorganic Chemicals*, McGraw-Hill, New York, 2003.

9 Q. Wang, J. Chen, K. Han, J. Wang and C. Lu, Influence of BaCO3 on chlorine fixation, combustion characteristics and KCl conversion during biomass combustion, *Fuel*, 2017, **208**, 82–90.

10 O. Dagdag, T. W. Quadri, R. Haldhar, S.-C. Kim, W. Daoudi, E. Berdimurodov, E. D. Akpan and E. E. Ebenso, An Overview of Heavy Metal Pollution and Control, C. V. Dakeshwar Kumar Verma, P. Kumar Mahish, *Heavy Metals in the Environment: Management Strategies for Global Pollution*, American Chemical Society, Washington, 2023, 3–24.

11 V. Singh, G. Ahmed, S. Vedika, P. Kumar, S. K. Chaturvedi, S. N. Rai, E. Vamanu and A. Kumar, Toxic heavy metal ions contamination in water and their sustainable reduction by eco-friendly methods: isotherms, thermodynamics and kinetics study, *Sci. Rep.*, 2024, **14**, 7595.

12 K. H. Hama Aziz, F. S. Mustafa, K. M. Omer, S. Hama, R. F. Hamarawf and K. O. Rahman, Heavy metal pollution in the aquatic environment: Efficient and low-cost removal approaches to eliminate their toxicity, *RSC Adv.*, 2023, **13**, 17595–17610.

13 R. Pandey, A. Kumar, Q. Xu and D. S. Pandey, Zinc (II), copper (II) and cadmium (II) complexes as fluorescent chemosensors for cations, *Dalton Trans.*, 2020, **49**(3), 542–568.

14 T. Gunnlaugsson, T. C. Lee and R. Parkesh, Highly selective fluorescent chemosensors for cadmium in water, *Tetrahedron*, 2004, **60**(49), 11239–11249.

15 K. M. Dimpe, J. C. Ngila, N. Mabuba and P. N. Nomngongo, Evaluation of sample preparation methods for the detection of total metal content using inductively coupled plasma optical emission spectrometry (ICP-OES) in wastewater and sludge, *Phys. Chem. Earth, Parts A/B/C*, 2014, **76–78**, 42–48.

16 K. Klotz, W. Weistenhöfer and H. Drexler, Determination of cadmium in biological samples, H. S. Astrid Sigel, R. K. O. Sigel, *Cadmium: from Toxicity to Essentiality*, Springer, Dordrecht, 2012, 85–98.

17 J. Khan, Optical chemosensors synthesis and appplication for trace level metal ions detection in aqueous media: a review, *J. Fluoresc.*, 2025, **35**(2), 561–582.

18 S. Kuppusamy, S. K. Kumar, A. M. Mohan and P. Deivasigamani, Metal-organic framework and porous polymer monolith as ion-receptor carrier templates for the solid-state naked-eye sensing of ultra-trace Cr (III) from aqueous medium, *Surf. Interfaces*, 2023, **42**, 103418.

19 S.-H. Park, N. Kwon, J.-H. Lee, J. Yoon and I. Shin, Synthetic ratiometric fluorescent probes for detection of ions, *Chem. Soc. Rev.*, 2020, **49**, 143–179.

20 G. V. Kumar, R. Kumar, G. Thiruppathi, P. Sundararaj and A. Draksharapu, Indole-Derived Multi-Ion Chemosensor for Turn-On Fluorescence and Bio-imaging Detection of Zn^{2+}, Al^{3+}, and Fe^{3+} Ions, *J. Environ. Chem. Eng.*, 2025, 117828.

21 I. M. El-Sewify, A. Radwan, N. H. Elghazawy, W. Fritzsche and H. M. E. Azzazy, Optical chemosensors for environmental monitoring of toxic metals related to Alzheimer's disease, *RSC Adv.*, 2022, **12**, 32744–32755.

22 T. Cheng, Y. Xu, S. Zhang, W. Zhu, X. Qian and L. Duan, A highly sensitive and selective OFF-ON fluorescent sensor for cadmium in aqueous solution and living cell, *J. Am. Chem. Soc.*, 2008, **130**, 16160–16161.

23 G. Aragay, J. Pons and A. Merkoçi, Recent trends in macro-, micro-, and nanomaterial-based tools and strategies for heavy-metal detection, *Chem. Rev.*, 2011, **111**, 3433–3458.

24 A. Radwan, I. M. El-Sewify and H. M. E.-S. Azzazy, Monitoring of Cobalt and Cadmium in Daily Cosmetics Using Powder and Paper Optical Chemosensors, *ACS Omega*, 2022, **7**, 15739–15750.

25 S.-Y. Park, P. Ghosh, S. O. Park, Y. M. Lee, S. K. Kwak and O.-H. Kwon, Origin of ultraweak fluorescence of 8-hydroxyquinoline in water: photoinduced ultrafast proton transfer, *RSC Adv.*, 2016, **6**, 9812–9821.

26 A. Moghaddasfar, G. M. Ziarani and A. Badiei, Upcycling waste zirconia block dental powders: towards a facile and highly selective on-off optical probe for sensing Zn 2+ and Hg 2+ in aqueous media, *RSC Adv.*, 2025, **15**, 16164–16174.

27 B. Sreedhar, C. S. Vani, D. K. Devi, M. B. Rao and C. Rambabu, Shape controlled synthesis of barium

carbonate microclusters and nanocrystallites using natural polysachharide—gum acacia, *Am. J. Mater. Sci*, 2012, **2**, 5–13.
28 A. Sivakumar, S. S. J. Dhas, A. I. Almansour, R. S. Kumar, N. Arumugam, K. Perumal and S. M. B. Dhas, Sustainability of the crystallographic phase stability of the barium carbonate nanoparticles at dynamic shocked conditions, *Applied Physics A*, 2021, **127**, 901.
29 J. Chaney, J. D. Santillán, E. Knittle and Q. Williams, A high-pressure infrared and Raman spectroscopic study of BaCO3: the aragonite, trigonal and Pmmn structures, *Phys. Chem. Miner.*, 2015, **42**, 83–93.
30 P. Pasierb, S. Komornicki, M. Rokita and M. Rękas, Structural properties of Li_2CO_3–$BaCO_3$ system derived from IR and Raman spectroscopy, *J. Mol. Struct.*, 2001, **596**, 151–156.
31 R. Behura, P. Mohanty, G. Sahu, P. P. Dash, S. Behera, R. Dinda, P. R. Hota, H. Sahoo, R. Bhaskaran, A. K. Barick, P. Mohapatra and B. R. Jali, A highly selective Schiff base fluorescent sensor for Zn^{2+}, Cd^{2+} and Hg^{2+} based on 2, 4-dinitrophenylhydrazine derivative, *Inorg. Chem. Commun.*, 2023, **154**, 110959.
32 Y.-P. Zhang, W.-Y. Niu, C.-M. Ma, Y.-S. Yang, H.-C. Guo and J.-J. Xue, Fluorogenic recognition of Zn^{2+}, Cd^{2+} by a new Pyrazoline-based Multi-Analyte chemosensor and its application in live cell imaging, *Inorg. Chem. Commun.*, 2021, **130**, 108735.
33 P. Muralakar, S. Ravi, P. Gayathri, S. Abraham, B. Jebasingh, S. P. Anthony, C. Ebenezer and R. V. Solomon, Highly Selective Turn-on Fluorescence Sensor for Cd^{2+} Ions by Tripodal Organic Ligand, *J. Fluoresc.*, 2024, **34**, 1229–1240.
34 S. Enbanathan and S. K. Iyer, A novel phenanthridine and terpyridine based D-π-A fluorescent probe for the ratiometric detection of Cd^{2+} in environmental water samples and living cells, *Ecotoxicol. Environ. Saf.*, 2022, **247**, 114272.
35 J. R. Bhamore, A. R. Gul, S. K. Kailasa, K.-W. Kim, J. S. Lee, H. Park and T. J. Park, Functionalization of gold nanoparticles using guanidine thiocyanate for sensitive and selective visual detection of Cd^{2+}, *Sens. Actuators B: Chem.*, 2021, **334**, 129685.
36 H. H. Cho, J. H. Heo, D. H. Jung, S. H. Kim, S.-J. Suh, K. H. Han and J. H. Lee, Portable Au Nanoparticle-Based Colorimetric Sensor Strip for Rapid On-Site Detection of Cd^{2+} Ions in Potable Water, *Biochip J*, 2021, **15**, 276–286.
37 Z. Yan, W. Yao, K. Mai, J. Huang, Y. Wan, L. Huang, B. Cai and Y. Liu, A highly selective and sensitive "on–off" fluorescent probe for detecting cadmium ions and L-cysteine based on nitrogen and boron co-doped carbon quantum dots, *RSC Adv.*, 2022, **12**, 8202–8210.
38 Y. Liu, X. Tang, M. Deng, T. Zhu, L. Edman and J. Wang, Hydrophilic AgInZnS quantum dots as a fluorescent turn-on probe for Cd^{2+} detection, *J. Alloys Compd.*, 2021, **864**, 158109.
39 J. Zhu, L. Fan, W. Li, X. Qi, C. Sun, W. Li and Z. Chang, A novel Eu-MOF ratiometric fluorescent probe for visual detection of Hg^{2+}, Cd^{2+} and formaldehyde, *J. Photochem. Photobiol.*, 2024, **452**, 115583.
40 A. P. De Silva, H. N. Gunaratne, T. Gunnlaugsson, A. J. Huxley, C. P. McCoy, J. T. Rademacher and T. E. Rice, Signaling recognition events with fluorescent sensors and switches, *Chem. Rev.*, 1997, **97**, 1515–1566.
41 S. Paul, R. Das and P. Banerjee, Recent endeavours in the development of organo chromo-fluorogenic probes towards the targeted detection of the toxic industrial pollutants Cu^{2+} and CN^{-}: recognition to implementation in sensory device, *Mater. Chem. Front.*, 2022, **6**, 2561–2595.
42 J. Tauc, R. Grigorovici and A. Vancu, Optical properties and electronic structure of amorphous germanium, *Phys. Status Solidi B*, 1966, **15**, 627–637.